ISABE-2015-20230

INVESTIGATIONS OF MULTIPLE SWIRL-VENTURI FUEL INJECTOR CONCEPTS: RECENT EXPERIMENTAL OPTICAL MEASUREMENT RESULTS FOR 1-POINT, 7-POINT, AND 9-POINT CONFIGURATIONS

Yolanda R. Hicks, Robert C. Anderson, Sarah A. Tedder, Kathleen M. Tacina
NASA Glenn Research Center
Cleveland, Ohio 44135 USA

Abstract

This paper presents results obtained during testing in optically-accessible, JP8-fueled, flame tube combustors using swirl-venturi lean direct injection (LDI) research hardware. The baseline LDI geometry has 9 fuel/air mixers arranged in a 3 × 3 array within a square chamber. 2-D results from this 9-element array are compared to results obtained in a cylindrical combustor using a 7-element array and a single element. In each case, the baseline element size remains the same. The effect of air swirler angle, and element arrangement on the presence of a central recirculation zone are presented. Only the highest swirl number air swirler produced a central recirculation zone for the single element swirl-venturi LDI and the 9-element LDI, but that same swirler did not produce a central recirculation zone for the 7-element LDI, possibly because of strong interactions due to element spacing within the array.

Nomenclature

Symbols

C_2^*	[-]	diatomic carbon radical
CH^*	[-]	CH radical
f	[mm]	focal length, f number
L/D	[-]	length-to-diameter ratio
NO_x	[-]	oxides of nitrogen
P	[kPa]	pressure
P_3	[kPa]	inlet combustor pressure
T	[K]	temperature
T_3	[K]	inlet combustor temperature
$\Delta P/P$	[-]	combustor pressure drop
Φ	[-]	equivalence ratio

Abbreviations

CFD	Computational Fluid Dynamics
FWHM	Full Width Half Maximum
(I)CCD	(Intensified) Charge-Coupled Device
LDI	Lean Direct Injection
Nd:YAG	Neodymium: Yttrium Aluminum Garnet
PIV	Particle Image Velocimetry
PLS	Planar Laser Scatter
UV	Ultraviolet

Introduction

Lean direct injection (LDI) is a low-NOx combustion concept in which the combustor operates fuel-lean, without a rich front end. LDI has seen on-going development under several NASA programs for its proven potential[1-4] to reduce fuel burn and reduce emissions. The drive toward improved engine efficiency has led to smaller cores and higher operating pressures, and the LDI research that was geared toward the High Speed Research program of the 1990s (LDI-1) is relevant in newer programs (LDI-2 and LDI-3) as regulations become increasingly stringent under both national and international guidelines.

Like other lean burn combustor concepts, LDI reduces NO_x by minimizing flame temperature; in fuel lean combustion, NO_x is an exponential function of temperature. To eliminate local "hot spots" that produce high levels of NO_x, lean burn combustion concepts rely on the fuel and air being well-mixed before burning occurs. Thus, LDI requires rapid fuel vaporization and fuel-air mixing. LDI achieves this by using a multi-element concept in which several small fuel/air mixers replace a single conventional fuel/air mixer.

Improved understanding of LDI operation will permit guideline development for future LDI combustor refinement. In order to achieve this understanding, examination of the physical and chemical processes that occur is required.

In the past, detailed optical measurements were acquired in a medium-pressure (2026-kPa) flame tube at NASA Glenn Research Center[5-9]. Unfortunately, test time in this medium pressure flame tube is limited. Therefore, NASA Glenn Research Center recently built a lower pressure (5-atm) flame tube designed specifically to facilitate combustor hardware testing, along with optical diagnostics measurements. This new 5-atm flame tube also allows for more frequent

configuration changes of the injector hardware to examine effects of injector offset or venturi throat length, for example. Because the maximum pressure ratio in the facility is 5, not all of the important non-dimensional parameters can be matched to anticipated next-generation flight operating envelopes. However the reference velocities and equivalence ratio can be matched, as well as the inlet temperatures and fuel pressures below 86% engine power.

This paper presents measurements for a 1-element swirl venturi LDI array to help elucidate the effect of air swirl angle and fuel nozzle distance relative to the venturi throat; and for a 7-element array to examine element interaction. Measurements of velocity, fuel injector patternation and flame chemiluminescence are presented. Results that compare fueling all elements to fueling only the center element are presented here. Results comparing the 1-point with just center fueling are shown for the first time. These are compared to one another and to previous 9-point results.

Experimental Setup

A. LDI configurations

The baseline configuration of the swirl-venturi LDI with axial air swirlers is that used in the 9-pt array (Fig. 1), described by Tacina et al[1]. The baseline element has a nominal 1-inch diameter. The axial distance from the swirler entrance to the combustor dump plane is about 1-inch, and the swirler vane angle is 60°, with all elements oriented to generate clockwise swirl downstream. Other air swirlers used were 45° and 52.5°. The swirlers consist of six-helical blades, and the outer diameter is approximately 0.875-inch. The converging-diverging venturi has no throat length. The fuel nozzle used is a hollow cone pressure-swirl atomizer positioned at the leading edge of the venturi throat. The nozzle is sized to have a flow number to provide nominally 10:1 turndown at the air flow rates appropriate to the facility operational envelope. Thus, the 9-pt nozzle has FN_{US} about 2.2; the 1-pt and 7-pt FN_{US} is about 0.7. The nozzles produce a hollow cone spray with spray angle near 70°. Common features between the three LDI configurations are that the fuel nozzles all have the same outer dimensions, and that the same air swirlers are used. The 1-point LDI has physically the same characteristics as the baseline configuration, with the exception that the venturi has a throat length of 0.061-in. The 7-point LDI element also has a throat length of 0.061-in; the other difference from the baseline for the 7-point is the overall length of about 0.82-in.

The LDI test hardware consisted of three basic arrangements, depicted in Fig. 2: first, a 3 x 3 array, referred to as the 9-point, with adjacent elements spaced 25.4-mm apart, and those on the diagonals separated by 35.9-mm; second, a 7-point, which is a circular array arranged with a center element surrounded by six outer elements, and each injector is 23.8-mm from any adjacent element; and third, a single LDI or 1-point, which is set up like the 7-point, with the outer six elements replaced by a screen designed to match the pressure drop the across those outer six elements. One other feature of the 1-point hardware is that the fuel nozzle tip can be positioned at different displacements upstream with respect to the venturi throat to examine its effect on the flow field, as illustrated in Fig. 3, which shows a cross section of the single LDI module.

Table 1 summarizes the key LDI element parameters and arrangements for the 1-point, 7-point, and 9-point LDI configurations.

B. Test Facilities

Two facilities that supply non-vitiated air were used to conduct the tests. Each provides optical access immediately downstream of the fuel injection site for non-intrusive optical and laser-based techniques to measure chemical and physical processes during multiphase combustion. Figure 4 has illustrations that highlight the optical access and basic arrangement for imaging experiments conducted in the two facilities.

The 9-point LDI was tested in the Combustor Subcomponent Test Facility, which features a high temperature and high pressure flame tube combustor rig. Flow passes horizontally in the facility. The test cell supplies non-vitiated inlet air to the combustor at temperatures between 505K and 866K, pressures between 1034-kPa and 1724-kPa with flow rates up to 4.54 kg/s. The combustor liner is formed using a castable ceramic to withstand average temperatures reaching 2033 K. UV-grade fused silica windows (38.1-mm axial × 50.8-mm) are mounted just downstream of the fuel injection site and provide optical access to the primary reaction zone, typically from three sides of the square combustion chamber. The chamber cross section measures 76.2-mm × 76.2-mm. Nitrogen film cooling is used internally to regulate window temperature and accounts for no more than 10% by mass of the total inlet air flow.

The 7-point and 1-point LDI experiments were conducted in the Combustion and Dynamics Facility (CDF), which is oriented vertically, with the flow through the combustor passing from top to bottom. The CDF can supply non-vitiated air preheated up to 810 K at air flow rates up to 0.35 kg/sec and pressures up to 517-kPa. The combustor test section is 15-cm long and has a circular cross-section nominally 7.62-cm in diameter (including the ceramic flame spray coating on the inner circumference). Three sets of

double-paned windows, spaced 90° apart around its circumference, are used to gain optical access to the water-cooled combustor. The windows are flat and have a small offset away from the combustor circumference. The windows measure 6.1-cm tall (axial direction) by 5.8-cm wide (azimuthal).

C. Diagnostic Setup—Imaging using Luminescence, 2-D PIV and PLS

All experiments used a layout similar to that illustrated in Fig. 4. For PIV and PLS, a laser beam was formed into a light sheet using a set of cylindrical lenses. The sheet was passed through the test section and aligned parallel with the flow direction. For chemiluminescence measurements, the camera was positioned so that the center plane of the test rig was in focus.

Chemiluminescence images of CH* were obtained using a gated, 16-bit, 1k × 1k pixel array, intensified CCD (ICCD) camera having a Gen II Super-Blue-Slow-Gate intensifier. Collection optics included a 430-nm bandpass filter (FWHM of 10-nm, typical) attached to a UV-grade, f = 105-mm, f/4.5, macro camera lens. We averaged 600 gates on-chip.

Movies of flames were achieved using a 12-bit, high speed CMOS camera (1k × 1k) focused on the vertical center plane. The light collected was largely a combination of CH* and C_2* emissions, emitted from the volume and within the field-of-view of the collection optics. For the 9-point work presented here, we used a frame rate of 10,000 frames per second, image exposure time of 40-µs, and image resolution of 576 × 944 pixels. The light was collected using an f = 150-mm, f/1.2 lens. For the 1-point work, the frame rate used was 30,000 frames per second (exposure time 33.3-µs or shorter), using an f = 60-mm, f/2.8 lens. The resolution was 512 x 352 pixels. For the 7-point tests, we framed at 40,000 per second (exposure time 25- µs or shorter), with resolution of 320 x 368 pixels, using an f = 50-mm, f/1.2 lens.

The PIV data were acquired using a 15-Hz double-head, frequency-doubled, Nd:YAG laser and a single, interline transfer, CCD camera. For the un-fueled, air-only tests (9-point only), 0.7-micron diameter alumina particles were seeded into the air inlet plenum 10-L/D before the plenum exit. The inlet plenum feeds the flow to the flame tube test section. For combusting experiments, seed was not used. Instead, we collected the light scattered by fuel particles to measure the liquid phase velocity. We used a mechanical leaf shutter to block light from the luminescent flame.

For the 1-point and 7-point tests, 2D, cold-flow PIV measurements were conducted using water or fuel from the nozzle as the light-scattering particles. In addition to standard PIV, we used planar laser scatter (PLS) to visualize liquid drops at 30 kHz (1-point) and 40-kHz (7-point) frame rates and to develop limited pseudo time-series PIV. PLS images were acquired using a continuous wave Nd:YAG laser with a total power output of ~1.1 watts (1-point) or 2 watts (7-point). As with PIV, the laser beam was formed into a vertical sheet (approximately 40-mm high for water and 25-mm high for fuel), positioned along y = 0. The laser sheet entered via the 0° window and exited through the 180° window.

Results and Discussion

We begin with a brief 9-point LDI review, then describe the 1-point and 7-point results and compare.

A. 9-point LDI

Figures 5-7 show example results depicting flow structure and nascent speciation via CH* chemiluminescence for the baseline, 9-point LDI injector.

For these 9-pt tests, we used exclusively the 60° air swirlers. Earlier work[1] shows that while the 45° swirlers produced the lowest NOx emissions overall, the 60° swirlers had a wider range of stable operation. One explanation for this is that the existence of a central recirculation zone (CRZ) promotes flame stability; however, the CRZ also serves to increase residence time of the hot fluid within the zone, which leads to increased NOx.

In a CFD analysis, Ajmani et al[10,11] modeled the 9-point LDI and compared the flow field using 45° and 60° swirlers at conditions similar to those used in reference 1. The analysis showed that a CRZ forms for the 60° swirler but not for the 45° swirler. Instead, recirculation zones attached to the dome face between elements.

We know from previous 9-point PIV experiments that the 60° swirlers generate CRZs as shown in the example in Fig. 5 which shows PIV results from the center vertical plane. The inlet conditions were T_3 = 828K and P_3 = 1034-kPa. Flow is left to right. The average velocity (Fig.5a) and RMS velocity (Fig.5b) fields shown are the result of averaging 500 instantaneous fields. The velocity magnitudes are plotted as gray-scale contours, and the direction of fluid motion is given using arrows. The region immediately downstream of the injectors shows upstream motion and the region between the injectors has high downstream velocity. The velocity plot also shows the upstream recirculating eddy regions that exist between the injectors where the upstream and downstream regions shear. The black contour shows the boundaries of zero velocity that separate the central recirculation zones from the bulk downstream motion. The RMS plot shows that the greatest

variation in the air velocity occurs in the region between injectors, which is also where the turbulence intensity is highest, and where the greatest potential for mixing between the elements exists.

When burning with the 9-pt injector, we saw that with all injectors fueled evenly at typical equivalence ratios (such as ϕ= 0.45 in Fig. 6), there was not much interaction between injectors in the near-field; flame CH* chemiluminescence shows that the primary flame zone is contained within the projected downstream boundaries of each element. Time series processing of the high speed images (Fig. 7a) also shows the burning flow structure has distinct regions—therefore, little interaction is seen between the elements. We found this to be the case regardless of the inlet temperature or combustor pressure.

For cases with only the center injector fueled (Figs. 6b,7b), the region near the dump plane is locally fuel-rich, with about thrice the amount of fuel compared to when all are fueled. Some of that excess fuel is transported into the high-velocity region between injectors where it can mix. (The flow lines downstream in Fig. 7b, track with the air-only stream lines in Fig. 5). Despite this, we determined[9] that the presence of the adjacent swirlers helps to confine the fuel spray to the region bounded by the high downstream air velocity around each element.

B. 1-point LDI

Using the single LDI, we explored the effect of air swirler angle on the combustor flow field and also on combustor operability. We used PIV and PLS to examine the non-combusting velocity field and examine injector patternation results in situ. In all cases, the "seed" was either water or fuel spray from the nozzle.

Figure 8 shows 1-point LDI PIV results for water spray. The air pressure, temperature, and flow rate were 517.1-kPa, 700K, and 0.107 kg/s, and the water flow rate was 3.89 kg/h. The fuel nozzle tip was at the venturi throat. The results shown are typical, and representative of all flow rates, air temperatures, and rig pressures used. Flow passes from top to bottom. The vectors show the direction of flow and the contour is colored by the axial velocity. The flow field generated by all swirlers shows a vector field which has positive-going velocity in a conical envelope, outside of which there is stagnant or reverse-going flow. The 45° swirler field has the fastest stream-wise velocity contained within a small region immediately downstream of the swirler exit and with size on the order of the LDI element, i.e., about 25-mm diameter. The minimum axial velocity is ~10-m/s. The field produced using the 52.5° swirler is similar to the 45° swirler, but with slightly lower maximum velocity spread out over a slightly larger region in space. The 60° swirler field is substantially different. It is the only one with a CRZ. The flow structure looks like a hollow cone; the maximum axial velocity is lowest; and the vectors near the exit make at least a 45 angle with respect to the centerline, whereas the angle for the 45° and 52.5° swirlers are on the order of 20 – 30 degrees. Also of note is that the spray takes up a larger volume compared to that for the 9-point injector. This might be because there are no swirlers adjacent; so operating the 7-point injector will help answer that question.

We measured the spray pattern and spray angle using the high-speed images of PLS. For each condition we randomly selected and analyzed 1000 high-speed image frames using IDL[12] and software[13] which finds and measures roughly circular features within an image. For each of the features, a radius and angle relative to the vertical measured from the dome exit at the injector centerline were determined. Spray pattern histograms were developed by creating software "bins" which were 3° wide with a radius that ranged from 10 to 30 mm. The software counted the features found in each bin throughout the 1000 frames analyzed. Using the droplet distribution histograms, we define the spray angle as the difference between the bin angle where the total count reached 5% and the angle where the count reached 95%. The trend in Fig. 7 closely matches the trends observed in the PIV velocity field in Fig. 5 (increasing spray angle with increasing swirler angle).

Figure 9 shows a histogram, computed as described above, for each swirler angle that reflects the angular spray distribution for droplets between 10-mm and 30-mm from the dump plane at r = 0. All three air swirlers show a bimodal distribution. For the 45° swirler, droplets are predominantly distributed ± 35°, with very few drops at smaller angles; the distribution reflects a hollow cone spray. As the swirler angle widens, more drops are distributed within the conical region—an indication that droplets have been entrained in the CRZ—and the angle at which drops occur widens. Qualitatively, there also is a larger number of droplets as the swirler angle increases; the larger swirler angles promote better spray atomization.

Figure 10 shows how the injector tip location affects the spray pattern when the tip is at (a) the venturi throat; (b), 0.16 throat diameters upstream; and (c), 0.31 throat diameters upstream. At its farthest upstream position, 0.31, the pattern is most clearly bimodal, whereas when at the venturi throat, the region directly downstream, within the conical region is almost completely filled in.

In terms of operability, although we could burn using the 52.5° swirler, we found it very difficult to light the combustor and maintain a stable flame. For the 60° swirler, we were able to light, and burn at a variety of conditions, for reference velocities ranging from 15-30 m/s, pressures from 200-517 kPa, inlet temperature ~715K, air flows from 0.068-0.27 kg/s, and local equivalence ratios from 0.5 to 2.0.

C. 7-point LDI

To examine the effect of adjacent elements, we ran the 7-point at the same inlet conditions as the 1-point LDI, fueling only the center element. Figure 11 shows the mean 2-D velocity field, when flowing water through the center. As with the 1-point LDI with the 60° swirler, we see the location of the high-velocity conical jet, which has a distinguishable, finite thickness, and a lower-velocity region downstream; however, the overall angle between the wings of the cone is smaller, and they converge in the middle. We did not see a CRZ, nor any other regions of reverse flow, at any flow condition.

The comparable droplet patternation for the same air conditions, but slightly higher ϕ are shown for water and fuel in Fig. 12. Most of the water spray is deposited within ± 40°, with nearly equal probability within that range. The high speed PLS images (Fig. 13) show a narrow spray of roughly 40° that wobbles somewhat irregularly from one side to the other. Alternately, one side or the other of the cone spray deposits its fluid near the centerline; hence, the spray pattern observed. No water is seen to move upstream. This is distinctly unlike the 1-point LDI (Fig.8c) which had a wide spray angle; the edges of the spray never approached the element centerline; and droplets could be seen to move upstream. 1-point LDI precession was also regular, with a frequency of ~1.1-kHz. For the 7-point, it seems the precessing vortex core frequency varies between 40-Hz and 100-Hz.

One possible reason for not seeing any recirculation for the 7-point LDI may be our reliance on using the water or fuel droplets as the seed for both the PIV and PLS measurements. If the droplets do not atomize well, then the measurements will be biased toward larger drops, which will not follow the air flow. Even if this is the case, we still observe that there is an effect of the outer swirlers on the center element, when compared to the 1-LDI case.

We think there is much more interaction between the adjacent elements for the 7-point LDI than for the 9-point, particularly since the element spacing is smaller, at 93% of the minimum 9-point spacing. Some studies have shown the effects of element spacing for swirl injectors. Kao[14,15] looked at the flow field interactions for 3- and 5-element linear arrays of radial-radial swirler elements. For swirler spaced of 1.75 and 2 diameters apart, they found the elements adjacent to the center element interacted to weaken the center element CRZ (CRZ strength alternated, so for the 5-element array, the pattern was weak-strong-weak-strong-weak). For larger spacings—2.5 and 2.75 diameters—the behavior was reversed and the center swirler CRZ was the stronger than the adjacent swirlers; thus for the 5-cup array, the pattern was strong-weak-strong-weak- strong. Work for which the spacings were on the order of the swirler diameter were described in the earlier section, on the 9-point.

Summary and Future Work

In this paper, we have presented recent measurements taken in an optically-accessible, JP8-fueled, flame tube combustor using 1-point and 7-point lean direct injection (LDI) research hardware, and compared them to the baseline 9-point array. Using PIV and high repetition rate planar laser scatter, we compared the flow fields using three air swirler angles (swirl number) to determine whether a central recirculation zone forms for the single point. We saw a CRZ for the 60° swirler case only. In running the 7-point LDI with the 60° swirlers, we did not see a CRZ. This may be because there is strong interaction between the elements, possibly because the spacing between elements is quite close. In future work, we plan to modify the injector spacing and element size.

Acknowledgment

This work was supported by the Transformational Tools and Technologies Project in NASA's Aeronautics Research Mission Directorate.

The authors gratefully thank the test crew: Brian Kramer, Kurt Rusmisel, Robert Bickford, Alan Revilock, Aimee Bogner, and Donald Hammett.

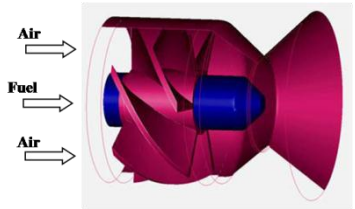

Figure 1. Schematic drawing that shows the relative spatial positions of the air swirler, fuel nozzle, and venturi for each LDI injector element.

Table 1. Key parameters of three SV-LDI configurations. Dimensions in inches.

	9-pt	1-pt	7-pt
Combustor flow passage dimension	3-in x 3-in	3 inch diameter	3 inch diameter
Element arrangement: array	3 x 3	1, centered, with surrounding screen	Center + 6 outer, 60° apart
Element size:			
Axial	1	1	0.82
Radial	0.873	0.873	0.873
Diffuser diameter at dump plane	0.875	0.875	0.800
Diffuser length	0.215	0.215	0.172
Element spacing, center-to-center of adjacent	1 or 1.414, position-dependent	n/a	0.938-
Venturi throat length	0	0.061	0.061
Venturi throat diameter	0.512	0.512	0.512

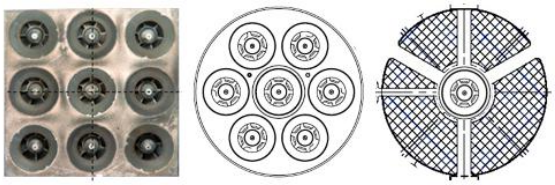

Figure 2. Aft-looking-forward views of the 9-point (left), 7-point (middle), and 1-point (right) LDI test hardware.

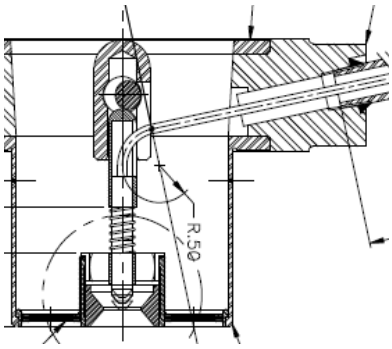

Figure 3. Detail showing positional variability of fuel nozzle relative to venturi throat for the 1-point SV-LDI.

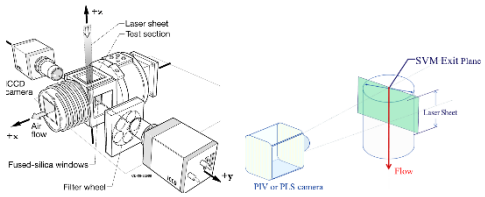

(a) (b)

Figure 4. Illustrations showing flame tube shape, general orientation, and window access used for typical 2-D imaging experiments: a) 9-point LDI, with laser sheet passing through the flow vertically; b) 1-point and 7-point LDI, with laser sheet travel horizontal tests.

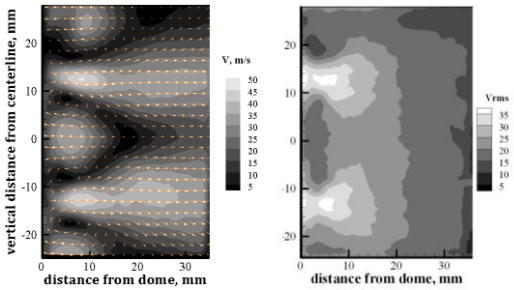

(a) (b)

Figure 5. Average velocity field (left) and RMS of velocity (right) within the vertical center plane, computed from 500, 2-D image pairs. T_3 = 828K, P_3 = 1034-kPa. Flow left to right.

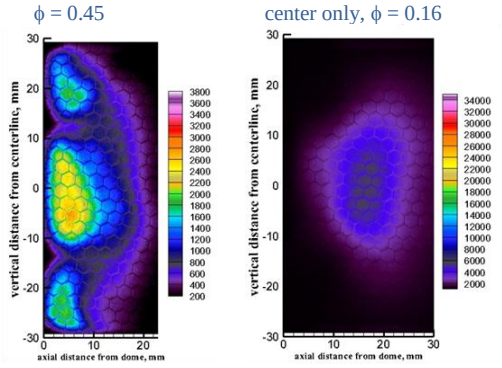

(a) (b)

Figure 6. On-chip integrated averages of CH at T_3 =617K. Left: ϕ = 0.45, evenly fueled. Right: center-only fueled, with ϕ_{local} = 1.45 and ϕ_{total} = 0.16. Flow is left to right.*

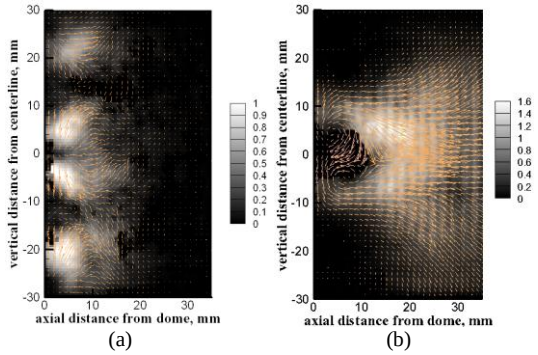

Figure 7. Average Flame/Flow structure derived using PIV-type processing of 9000 consecutive high-speed image pairs. T_3 = 828K. Left: Nine injectors fueled equally. Right: Center injector fueled only.

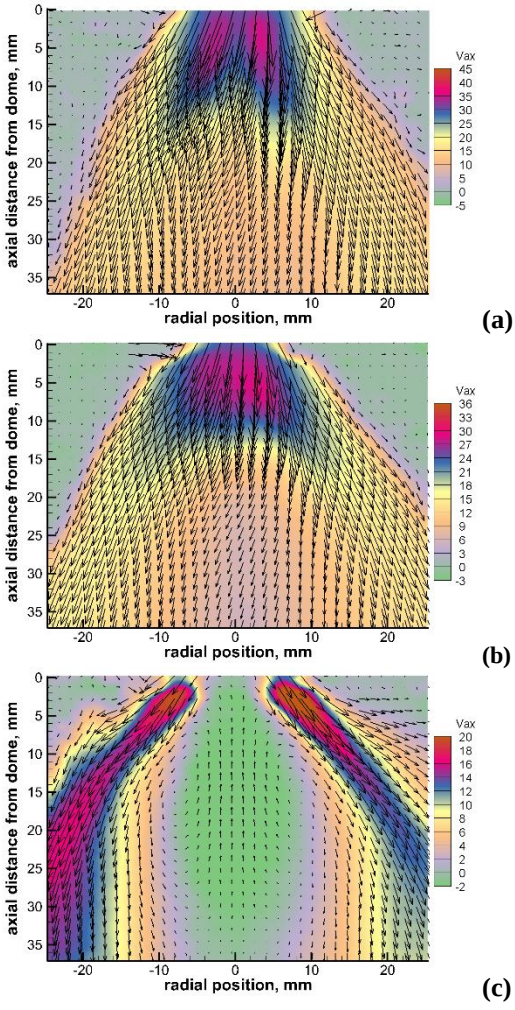

Figure 8. 1-point LDI. PIV average velocity fields in center plane for water spray with injector tip at the venturi throat. T_3 = 700K, P_3=217.1-kPa, air flow rate = 0.107 kg/s, reference velocity= 9.1 m/s, water flow rate= 3.89 kg/h. Increasing air swirler angle from left to right: (a) 45 degrees, (b) 52.5 degrees, (c) 60 degrees. The flow is from top to bottom.

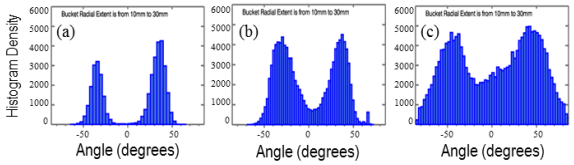

Figure 9. Occurrences of droplets at angles relative to center of air mixer exit with injector tip at the venturi throat. T_3 = 700K, P_3=217.1-kPa, air flow rate = 0.107 kg/s, reference velocity= 9.1 m/s, water flow rate= 3.89 kg/h. Air swirler: (a) 45º, (b)52.5º, (c) 60º.

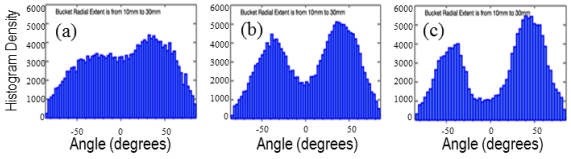

Figure 10. Occurrences of droplets at angles relative to center of air mixer exit with injector tip at the venturi throat. T_3 = 700K, P3=217.1-kPa, air flow rate = 0.143 kg/s, reference velocity= 12.2 m/s, water flow rate= 4.09 kg/h. Injector tip distance upstream of the throat in throat diameters: (a) 0, (b) 0.16, (c) 0.31

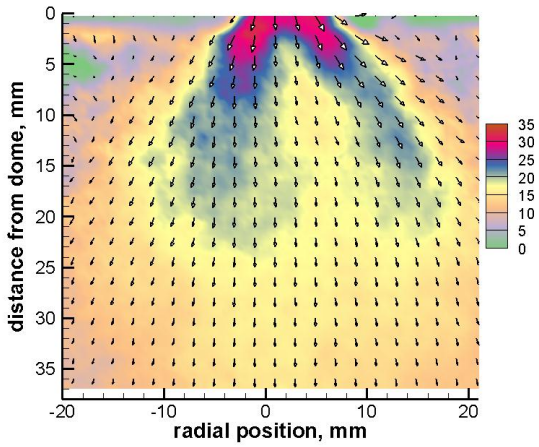

Figure 11. 7-point LDI: Average PIV velocity fields at vertical center plane for water spray, liquid from center nozzle only. T_3 = 650K, P_3=217.1-kPa, air flow rate = 0.107 kg/s, reference velocity= 9.1 m/s, water flow rate= 3.89 kg/h. The flow is from top to bottom.

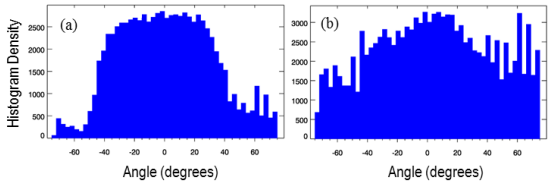

Figure 12. Drop Occurrences at angles relative to center of air mixer exit for liquid through the 7-point LDI center element and no flow to the outer elements. T_3=650K, P_3=217.1-kPa, air flow rate = 0.107 kg/s, reference velocity=9.1 m/s. (a): water flow, at 7.01 kg/h; (b): JP-8, at 5.65 kg/h.

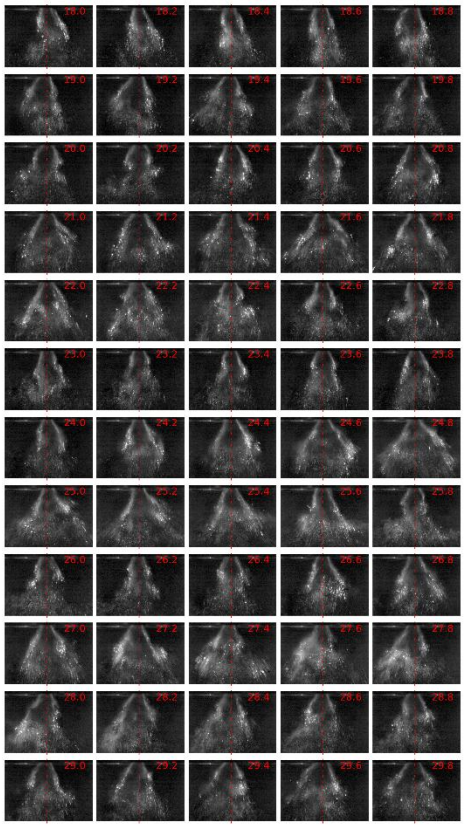

Figure 13. Individual movie frames from center-only "fueling" using water in the 7-point LDI. T_3 = 650K, P_3=217.1-kPa, air flow rate = 0.107 kg/s, reference velocity= 9.1 m/s, water flow rate= 3.89 kg/h. Flow from top to bottom.

References

[1]Tacina, R., Lee, P., and Wey, C., "A Lean-Direct-Injection Combustor Using a 9 Point Swirl-Venturi Fuel Injector", ISABE-2005-1106, 2005.

[2]Wey, C. and Bulzan, D., Effects of Bio-Derived Fuels on Emissions and Performance Using a 9-Point Lean Direct Injection Low Emissions Concept," GT2013-94888, 2013.

Lee, C.-M., Chang, C., Kramer, K. and Herbon, J. T., "NASA Project Develops Next Generation Low-Emissions Combustor Technologies," AIAA-2013-0540.

[4]Tacina, K.M., Chang, C.T. and He, Z.J., "A Second Generation Swirl-Venturi Lean Direct Injection Concept," AIAA-2014-3434.

[5]Locke, R.J, Hicks, Y.R, and Anderson, R.C., "Combustion Imaging Using Fluorescence and Elastic Scattering," *Optical Metrology for Fluids, Combustion, and Solids*, edited by C. Mercer, Kluwer Academic Publishers, Norwell, MA, 2003, pp. 175-208.

[6]Hicks, Y.R., Locke, R.J., and Anderson, R.C., "Optical Measurement and Visualization in High-Pressure, High-Temperature, Aviation Gas Turbine Combustors", *Optical Diagnostics for Industrial Applications*, edited by Neil A. Halliwell, editor, Proceedings of SPIE Vol. 4076, 2000, pp. 66 – 77. Also published as NASA TM-2000-210377, 2000.

[7]Hicks,Y.R., Anderson, R.C., and Locke, R.J., "Optical Measurements in a Combustor Using a 9-Point Swirl-Venturi Fuel Injector", International Society for Air Breathing Engines, ISABE-2007-1280, 2007.

[8]Heath, C.M., Locke, R.J., Anderson, R.C., and Hicks, Y.R., "Optical Characterization of a Multipoint Lean Direct Injector for Gas Turbine Combustors: Velocity and Fuel Drop Size Measurements", IGTI, GT2010-22960, 2010.

[9]Hicks, Y.R., C.M. Heath, R.C. Anderson, and K.M. Tacina [2011]. "Investigations of a Combustor Using a 9-Point Swirl-Venturi Fuel Injector: Recent Experimental Results," Paper ISABE-2011-1106, NASA/TM-2012-217245.

[10]Ajmani, K., Mongia, H.C., and Lee, P., "Evaluation of CFD Best Practices for Combustor Design: Part I—Non-Reacting Flows," AIAA-2013-1144, 2013.

[11]Ajmani, K., Mongia, H.C., and Lee, P., "Evaluation of CFD Best Practices for Combustor Design: Part II—Reacting Flows," AIAA-2013-1143, 2013.

[12]IDL, *Exelis Visual Information Solutions, Software Package, Ver. 8.3, Boulder, Colorado, 2013.*

[13]Feature.pro, John C. Crocker and David G. Grier, Emory University, Atlanta, Ga, 1996.

[14]Kao, Y.-H., Tambe, S.B., and Jeng, S.-M., "Effect of Dome Geometry on Swirling Flow Field Characteristics of a Counter-Rotating Radial-Radial Swirler", IGTI, GT2013-95344, 2013.

[15]Kao, Y.-H., "Experimental Investigation of Aerodynamics and Combustion Properties of a Multiple-Swirler Array", Dissertation, University of Cincinnati, 2014.